THE JOURNAL OF BIOLOGICAL CHEMISTRY VOL. 285, NO. 6, pp. 4049–4059, February 5, 2010

Crystal Structure of Plant Ferritin Reveals a Novel Metal Binding Site That Functions as a Transit Site for Metal Transfer in Ferritin*

Received for publication, August 25, 2009, and in revised form, November 25, 2009 Published, JBC Papers in Press, December 9, 2009, DOI 10.1074/jbc.M109.059790

Taro Masuda[‡1], **Fumiyuki Goto**[§], **Toshihiro Yoshihara**[§], **and Bunzo Mikami**[¶]

From the [‡]*Laboratory of Food Quality Design and Development, Division of Agronomy and Horticultural Science, Graduate School of Agriculture, and the* [¶]*Laboratory of Applied Structural Biology, Division of Applied Life Sciences, Graduate School of Agriculture, Kyoto University, Gokasho, Uji, Kyoto 611-0011 and the* [§]*Biotechnology Sector, Environmental Science Research Laboratory, Central Research Institute of Electric Power Industry, 1646 Abiko, Abiko, Chiba 270-1194, Japan*

Ferritins are important iron storage and detoxification proteins that are widely distributed in living kingdoms. Because plant ferritin possesses both a ferroxidase site and a ferrihydrite nucleation site, it is a suitable model for studying the mechanism of iron storage in ferritin. This article presents for the first time the crystal structure of a plant ferritin from soybean at 1.8-Å resolution. The soybean ferritin 4 (SFER4) had a high structural similarity to vertebrate ferritin, except for the N-terminal extension region, the C-terminal short helix E, and the end of the BC-loop. Similar to the crystal structures of other ferritins, metal binding sites were observed in the iron entry channel, ferroxidase center, and nucleation site of SFER4. In addition to these conventional sites, a novel metal binding site was discovered intermediate between the iron entry channel and the ferroxidase site. This site was coordinated by the acidic side chain of Glu^{173} and carbonyl oxygen of Thr^{168}, which correspond, respectively, to Glu^{140} and Thr^{135} of human H chain ferritin according to their sequences. A comparison of the ferroxidase activities of the native and the E173A mutant of SFER4 clearly showed a delay in the iron oxidation rate of the mutant. This indicated that the glutamate residue functions as a transit site of iron from the 3-fold entry channel to the ferroxidase site, which may be universal among ferritins.

Ferritin is a class of iron storage proteins distributed ubiquitously in plants, mammals, and bacteria. This protein class plays an important role in storage and detoxification of excess iron in a living cell. Although the primary sequences of ferritins vary, their three-dimensional structures of 24 structurally equivalent subunits assembled into a cage-like oligomer and related by 4-, 3-, and 2-fold symmetry axes (1–3) are highly conserved. Each subunit has four helices (A-D), each of which is composed of ~30 amino acid residues, along with a fifth short helix (E) having 10 residues or more, resulting in the formation of a "four-helix bundle." In general, the outer shell diameters of the spherical oligomeric ferritin composed of 24 subunits are ~120 Å, whereas the inner cavity diameters are ~80 Å. Up to 4500 iron atoms are deposited in the inner cavity of ferritin (1–3). To date, three major metal binding sites have been identified in ferritin. These exhibit some common aspects related to the iron storage mechanism: (i) they exist around the 3-fold symmetry channel, (ii) constitute a ferroxidase center in the four-helix bundle, and (iii) constitute a nucleation site facing the inner cavity of ferritin (4–7). It has been suggested that iron atoms pass through the hydrophilic channels that traverse the ferritin shell around the 3-fold symmetry axes of oligomeric ferritin (8–11). This funnel-like channel is surrounded by hydrophilic residues, such as aspartic acid and glutamic acid, which have been demonstrated to serve as ligands for metal ions, such as ferrous, calcium, or zinc ions (4, 5). With respect to the ferroxidase center and nucleation center, two distinct subunits, heavy (H)[2] and light (L) chains, are seen in mammalian ferritin (12–14). The H chain possesses the ferroxidase site (15, 16), which is positioned inside the 4-helix bundle of each subunit and is responsible for oxidation of ferrous iron atoms to produce the μ-oxo-bridged Fe(III) species. The ferroxidase site is composed of six residues: Glu^{27}, Tyr^{34}, Glu^{62}, His^{65}, Glu^{107}, and Gln^{141}, which coordinate with metal ions directly or indirectly. Crystallographic analyses of ferritin in vertebrates (4, 5, 17), insects (18), and bacteria (7, 19) revealed an extremely high degree of similarity among the structures of these ferroxidase centers. On the other hand, the L-type ferritin lacks the ferroxidase center, but possesses the nucleation site. The site is composed of three or four glutamate residues facing the inner cavity of the ferritin shell, and facilitates ferrihydrite nucleation (20, 21). In mammals, the H and L chains form a heteropolymer and cooperatively share the role of iron storage *in vivo* (14).

Recently, multiple copies of the ferritin gene were identified from various plant species (22–30). It has been suggested that their expression was differentially regulated via various environmental stresses or metal overload (25, 31–36), and are sometimes subjected to different types of processing (26, 30). In contrast to the case of the H and L chains of mammalian ferritin, all of the identified plant ferritin subunits have similar primary sequences, especially in their deduced ferroxidase center and nucleation site. Although the primary structures of plant ferritins are basically well conserved with those of mammalian

* This work was supported a grant from the Shorai Foundation for Science and Technology (to T. M.).

The atomic coordinates and structure factors (codes 3A68 and 3A9Q) have been deposited in the Protein Data Bank, Research Collaboratory for Structural Bioinformatics, Rutgers University, New Brunswick, NJ (http://www.rcsb.org/).

[1] To whom correspondence should be addressed. Tel.: 81-774-38-3762; Fax: 81-774-38-3761; E-mail: masutaro@kais.kyoto-u.ac.jp.

[2] The abbreviations used are: H, heavy; L, light; EP, extension peptide.

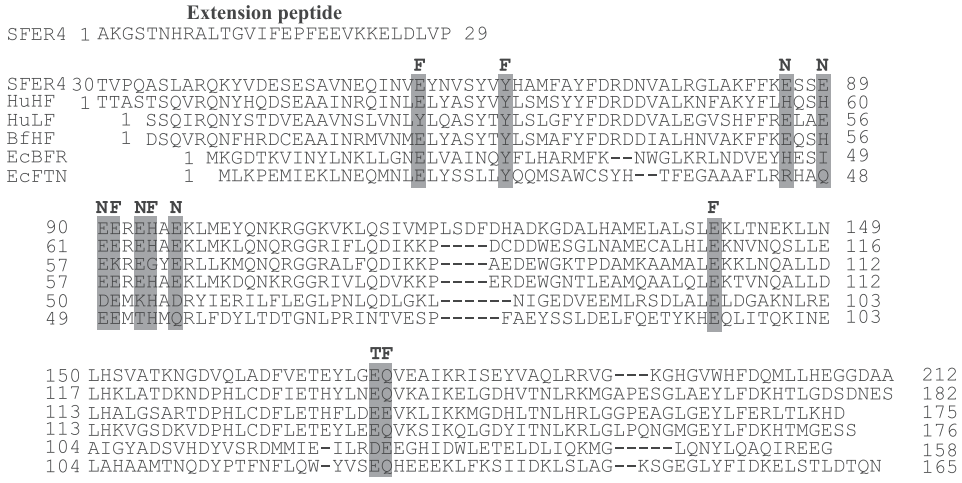

FIGURE 1. **Amino acid sequences of the plant ferritin, SFER4, and other ferritin from vertebrate and bacteria.** The sequences of SFER4 (GenBank number AB062756), human H (HuHF, M11146), human L (HuLF, M11147), bullfrog H (BfHF, M15655), and two *E. coli* ferritins (EcBFR (Swiss Prot P0ABD3) and EcFTN (GenBank number X53513)) are shown. Conserved ferroxidase center, putative nucleation center, and transit site discussed in this study are shown *boxed*. The letters *F*, *N*, and *T* on the *boxed sequences* indicate the ferroxidase site, nucleation site, and transit site, respectively.

ferritins (Fig. 1), plant ferritins show two further differences: first, plant ferritin possesses the N-terminal extension regions, which can be divided into two parts based on their functions (37). The upstream one is called a "transit peptide" responsible for transportation of the polypeptide chain to plastid, whereas the downstream one is called an "extension peptide" (EP) with an unknown function (38). Several reports have suggested that EP helps to stabilize the oligomeric protein shell (39–41). Second, plant ferritins can incorporate and store iron without the differentiation of subunits. As mentioned above, all plant ferritins possess both a ferroxidase center and a nucleation site. These observations led us to hypothesize that a crystallographic analysis of plant ferritin would offer new insight into the pathway of metal ion transfer from the iron entry channel via the ferroxidase center to the nucleation site and inner cavity of the ferritin shell. With respect to the three-dimensional structures of plant ferritin, Lobréaux *et al.* (42) presented the deduced structure of ferritin from pea (*Pisum sativum*) using a computer simulation. They predicted that the main chain structure of plant ferritin can be superimposed onto human H chain ferritin up to 1 Å of the root mean square distance (42). Thus, it can be considered that its overall structure, including structure of the 3-fold symmetry channel, ferroxidase center, and nucleation site, is highly conserved. However, the actual metal binding sites and precise orientation of side chains of metal ligands have remained unclear. On the other hand, we have attempted to crystallize plant ferritin from soybean (SFER1) to obtain the real structure of these active sites; however, the diffraction data from the crystal were not sufficient to provide high resolution structural analysis (43).

In this study, to address the question of the metal ion pathway in the ferritin oligomer, we have crystallized a recombinant plant ferritin subunit from soybean (SFER4). The high resolution x-ray crystallographic analysis of this soybean ferritin subunit has revealed a novel metal binding site between the 3-fold symmetry channel and ferroxidase center. The deletion of this site resulted in a delay of the iron oxidation/nucleation process, suggesting that this site functions as a transit site for metal translocation in ferritin. Based on these results, coupled with the extremely high conservation of this site, we propose that this site is part of the metal ion pathway widely distributed in ferritin from various species.

EXPERIMENTAL PROCEDURES

cDNA Cloning and Protein Preparation—Cloning of the soybean ferritin SFER4 cDNA (GenBank™ number AB062756) was performed as described previously (44). The SFER4 cDNA fragment containing NcoI and BamHI restriction sites was cloned into pET21d (Novagen, San Diego, CA) through restriction sites NcoI and BamHI using a PCR-based method. The E173A SFER4 variant was obtained by oligonucleotide site-directed mutagenesis using pET_SFER4 as a template. The DNA sequence of the resulting plasmid pET_SFER4 and pET_SFER4-E173A was verified by automated DNA sequencing (ABI PRISM 3100, Applied Biosystems, Foster City, CA). The constructs were then introduced into *Escherichia coli* strain BL21(DE3). The positive transformants of each construct were grown at 37 °C on LB medium supplemented with 50 mg/liter of carbenicillin, and protein expression was induced with 100 μM isopropyl β-D-1-thiogalactopyranoside when the cell density reached an A_{600} of 0.6. Eventually, the cells were harvested by centrifugation after 3 h of induction and resuspended in Buffer A (10 mM Tris-HCl, pH 7.5, 1 mM EDTA, 0.15 M NaCl, 0.1 mM *p*-amidinophenyl)methanesulfonyl fluoride hydrochloride, 0.2 μM pepstatin, 0.5 g/liter leupeptin) to a concentration of 40 g (fresh weight bacteria)/liter, followed by disruption by sonication. The supernatant of the resulting crude extract was collected by centrifugation and fractionated by 50–60% saturation of ammonium sulfate. The pellet was resuspended in Buffer B (20 mM Tris-HCl, pH 7.8, 1 mM EDTA) and dialyzed against the same buffer. The protein solution was applied to an ion-exchange column (Q-Sepharose 26/10, GE Healthcare, Piscataway, NJ), followed by elution with 0–0.5 M NaCl gradient. Finally, the protein solution was concentrated and purified on a gel filtration column (Superdex 200pg 16/60, GE Healthcare), equilibrated with Buffer C (10 mM Tris-HCl, 0.15 M NaCl). The resulting SFER4 and SFER4-E173A were electrophoretically pure (data not shown). The protein concentrations were estimated by A_{280}, using molar absorptivity (ϵ_M) of 17,420 cm^{-1} M^{-1}, calculated from amino acid composition (45).

Crystallization, Data Collection, and Processing—Initial crystals of native SFER4 were obtained after about 2 weeks (Wizard I; B-Bridge, Mountain View, CA) using the hanging drop vapor diffusion method. The optimized crystallization drops were prepared by mixing equal volumes of mother liquid

composed of 15% PEG 1000, 0.2 M calcium acetate, 0.1 M imidazole, pH 7.8, and protein solution containing 10 mg/ml of recombinant SFER4. Orthorhombic crystals of SFER4 (space group $P2_12_12$; a = 222.610, b = 220.886, c = 122.452 Å; V_M = 2.61 Å^3/Da for 24 monomers per asymmetric unit) of ~0.5 × 0.2 × 0.2 mm appeared within 3 weeks at 20 °C. The crystallization condition of the E173A variant was the same as that of the native crystal. Diffraction data of the native and E173A crystals were collected to 1.8- and 1.9-Å resolution at 77 K at the SPring-8 beamline 44XU after flash cooling with 30% of 2-methyl-2,4-pentanediol as a cryoprotectant. Data were processed, merged, and scaled with HKL-2000 (HKL Research, Charlottesville, VA) (46). Data processing statistics are shown in Table 1.

Structure Determination and Refinement—The structure of native SFER4 was determined by molecular replacement using the Molrep program (47) in CCP4i suit 1.4.4 (48) using the structure of bullfrog M ferritin (PDB code 1MFR) (17) as a search model. All water molecules and calcium atoms were removed from the search model prior to molecular replacement. Refinement was performed with 24-fold non-crystallographic symmetry using the REFMAC5 program (49) in CCP4i suit 1.4.4 (48). The structure was visualized and rebuilt using COOT 0.5.2 (50) and further modified on σ-weighted ($2|F_o|-|F_c|$) and ($|F_o| - |F_c|$) electron density maps. Water molecules were added using the COOT autofind function with a lower cutoff of 3 σ in the $|F_o| - |F_c|$ map. Metal ions were positioned into higher ($|F_o| - |F_c|$) residual densities and according to shorter bond distances with neighboring water molecules or other protein ligands. A Bijvoet difference Fourier map calculated from the final protein model was used to identify the metal binding sites. The final refinement was carried out using *PHENIX* software (51). The structure of the E173A variant was determined using the final model of the native SFER4, and the refinement strategy was the same as that for the native. Figs. 2–6 and 8 were produced by PyMOL (DeLano Scientific, San Carlos, CA).

Iron Uptake—Apoferritins of native SFER4 and the E173A variant were obtained using the methods described by Chasteen and Theil (52) with some modifications. Purified ferritins were dialyzed against 50 mM HEPES-Na buffer, pH 7.0, containing 1% thioglycolic acid, followed by successive changes of HEPES-Na buffer with (0.1%) or without thioglycolic acid. The protein was then dialyzed against Tris-HCl buffer containing 13 g/liter of Chelex 100 (Bio-Rad Laboratories) and 0.15 M NaCl, and finally dialyzed against 10 mM Tris-HCl, pH 7.5, containing 0.15 M NaCl. The concentration of purified proteins was determined using the absorbance at 280 nm.

Reactions examining iron uptake by native and the E173A variant were performed in 10 mM Tris-HCl, pH 7.5, containing 0.15 M NaCl with a Fe^{2+}/ferritin molar ratio of 100:1, 40:1, and 20:1 (100, 40, and 20 μM ferrous ammonium sulfate and 1 μM ferritin) at 25 °C. Iron oxidation/nucleation by each type of ferritin was monitored by measuring the absorbance at 310 nm, the generation of μ-oxo-bridged Fe(III) species (16, 54) using a UV spectrophotometer (UV160, Shimadzu, Kyoto, Japan), and the resulting absorbance every 10 s for kinetic analysis. After each Fe(II) addition, several spectra were taken until the absorbance increased no further. The molar absorptivity of 4570 (cm^{-1} M^{-1}), which was calculated for μ-oxo bridged Fe(III) in a iron excess condition on horse spleen ferritin by Yang *et al.* (21), was used to calculate the kinetic parameters. The kinetics data were analyzed with Excel 2007 software (Microsoft, Redmond, WA). The initial rates of iron oxidation were obtained from the linear A_1 term of a third-order polynomial fitted to the experimental data (21, 55). The kinetic parameters were calculated by Lineweaver-Burk plots.

Data Deposition—Coordinates of plant ferritin SFER4 and its variant E173A have been deposited at the RCSB Protein Data Bank with accession codes 3A68 and 3A9Q, respectively.

TABLE 1
Data collection and refinement statistics for the crystals of plant ferritin SFER4 and its variant E173A

	Native SFER4	SFER4 variant E173A
Data collection statistics		
Space group	$P2_12_12$	$P2_12_12$
Lattice parameter (Å)	a = 222.610, b = 220.886, c = 122.452	a = 223.494, b = 221.798, c = 122.705
Wave length (Å)	0.90	0.90
Resolution (highest shell) (Å)	50-1.8 (1.83-1.80)	50-1.9 (1.93-1.90)
No. unique reflections	546,597	473,818
Completeness (%)	98.9 (97.1)	99.2 (97.0)
Data redundancy	5.8 (4.6)	6.6 (5.9)
R_{merge}	0.058 (0.259)	0.102 (0.356)
$\langle I/\sigma(I)\rangle$	18.4 (7.96)	15.7 (8.34)
Refinement statistics		
Resolution (Å)	50-1.8	50-1.9
Number of amino acid residues	4,642	4,629
Number of atoms		
Protein	39,272	39,197
Solvent	4,570	3,429
Ca^{2+}	136	130
Acetate (No. of molecule)	72 (18)	72 (18)
R-factor	0.1423	0.1504
R_{free}	0.1727	0.1850
Root mean square deviation from ideality		
Bond length (Å)	0.004	0.006
Bond angle (deg.)	0.771	0.870
Average B-factor (Å^2)		
Main chain (Å^2)	15.85	16.74
Side chain (Å^2)	24.48	23.56
Water (Å^2)	26.48	23.64
Ca^{2+} (Å^2)	35.00	35.27
Acetate (Å^2)	37.38	37.74

RESULTS

Model Quality and Overall Structure of Plant Ferritin (SFER4) Subunit—The overall coordinate error of the final model, estimated from Luzzati plots, was 0.18 Å. Root mean square deviations of bond lengths and angles from ideality as calculated by the *PHENIX* program are listed in Table 1. These values are well within accepted limits, indicating that all of the structures have tight stereochemical constraints. A Ramachandran plot of the final structure showed that 98.43 and 1.57% of all residues were in the most favored and allowed regions, respectively. Refinement statistics are shown in Table 1.

The final model contained the whole oligomeric protein shell composed of 24 subunits with 4642 residues, 4570 waters, 136 Ca^{2+} ions, and 18 acetate ions. Like the structures of ferritins from vertebrates and bacteria, the structure of plant ferritin, SFER4, has a cage-like hollow shell composed of 24 subunits, which are related by 4-, 3-, and 2-fold symmetry (Fig. 2). There are four 3-fold axes and three 4-fold axes traversing the shell of

the assembled 24-mer, resulting in eight 3-fold channels and six 4-fold channels. In the present model for SFER4, each subunit excludes the N-terminal 11 to 13 residues and the C-terminal 5 residues, because they have no electron density. Exceptionally, chain E excludes the first 17 residues. The N-terminal EP (from the N terminus to Thr^{30} in this model) forms a loop and a short helix that lies on the C-helix in a neighboring 3-fold symmetry mate (counterclockwise) (Fig. 2*a*), although the side chains of amino acids in the region are relatively disordered and have high temperature factors (Fig. 2). The interactions between the EP and the conserved helical region of an adjacent chain were formed mainly by apolar contacts, except for an ion pair formed between Glu^{20} and Lys^{146}. Table 2 shows an example of side chains and residues related to the interactions between the EP of chain G and the helical region of chain O. The conserved region of each chain is composed of A-helix (from Asp^{43} to Asp^{71}), B-helix (from Arg^{78} to Arg^{105}), BC loop (from Gly^{106} to Gly^{127}), C-helix (from Asp^{128} to Asn^{157}), D-helix (from Val^{160} to Val^{191}), and E-helix (from His^{195} to Glu^{207}). The D-helix contains a typical kink at position Tyr^{170}, which is required to open the 3-fold channel. These backbones are highly conserved among ferritins with known structures. For example, when superimposing a single chain of the SFER4 on a human H chain (PDB code 2FHA) (4), the average root mean square distance between C^{α} was 0.95 Å. The large deviation, except for the N-terminal EP, was observed at the end of the BC and DE loops due to the insertion and deletion of 4 and 3 residues, respectively (Fig. 2*c*).

The model showed 136 metal ions. Most had 6–7 coordination bonds with weak significant anomalous signals. Thus, they were interpreted as calcium ions, which were contained in the crystallization solution. These calcium ions can be categorized into 5 groups. First, in

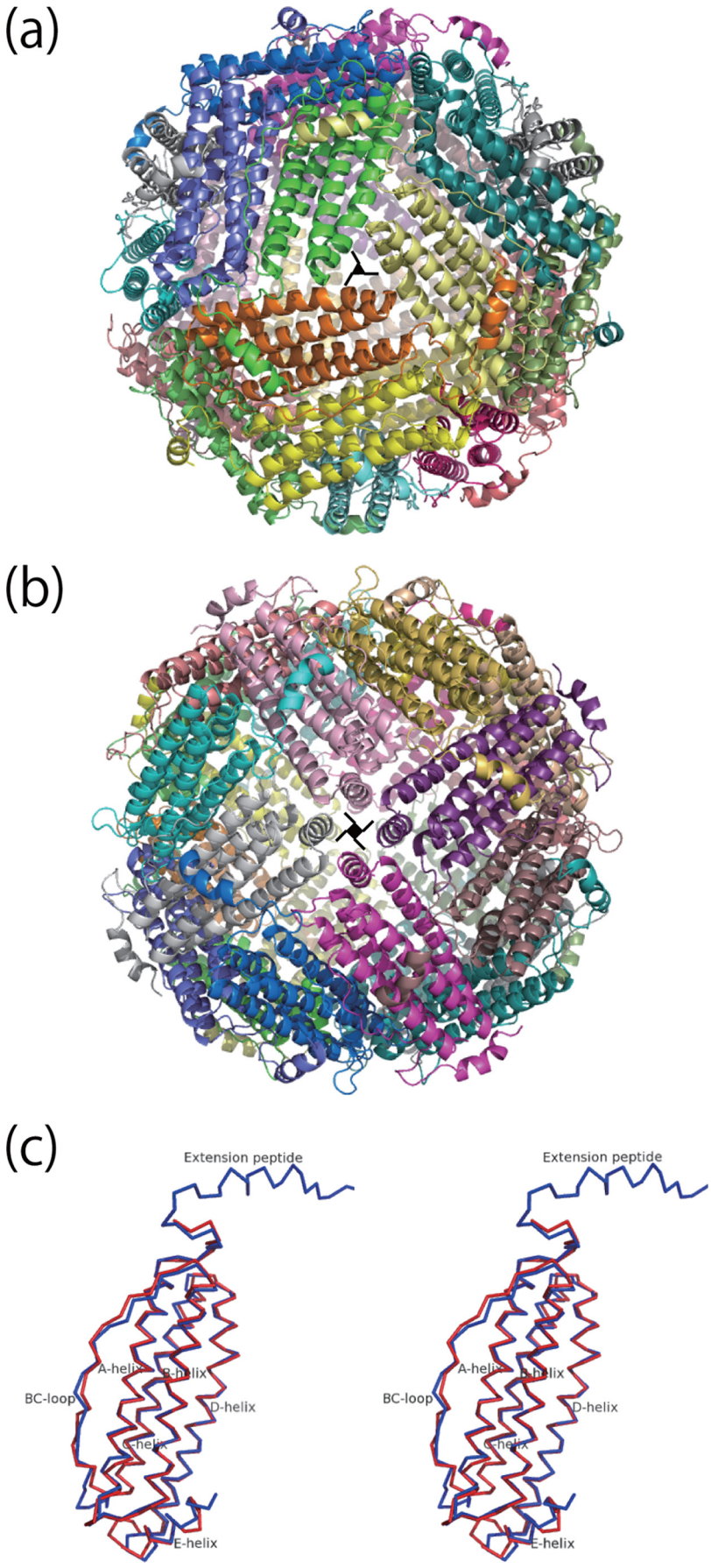

TABLE 2

Interactions between the extension peptide of the chain G and conserved helical regions of the chain O

The cutoff distances for C-C contacts and a hydrogen bonds are 4.20 and 3.25 Å, respectively.

Extension peptide	Conserved helical regions	Distances
		Å
Phe^{15} CZ	Leu^{142} (helix C) CD1	3.41
Phe^{15} CE1	Asn^{58} (helix A) CB	3.81
Phe^{15} CE2	Lys^{146} (helix C) CE	3.83
Pro^{17} CG	Val^{62} (helix A) CG3	4.13
Pro^{17} CB	Leu^{139} (helix C) CD1	4.00
Phe^{18} CE2, CZ	Val^{62} (helix A) CG2, CG1	3.80, 3.59
Phe^{18} CZ, CD1	Leu^{118} (BC loop) CB, CG	3.71, 3.68
Phe^{18} CE1	Leu^{135} (helix C) CD1	3.56
Glu^{20} CB	Leu^{142} (helix C) CD2	4.19
Val^{21} CG2	Leu^{139} (helix C) CD1	3.98
Leu^{25} CD2	Leu^{135} (helix C) CD2	3.84
Glu^{20} OE2	Lys^{146} (helix C) NZ	3.10 (charged hydrogen bond)

the outer surface of the ferritin molecule (22 Ca^{2+} ions); second, around the 3-fold symmetry channel deduced as an iron entry channel (18 Ca^{2+} ions); third, in the ferroxidase center located inside the 4-helix bundle (24 Ca^{2+} ions); fourth, on the inner surface of the ferritin shell containing two binding sites (48 Ca^{2+} ions); and fifth, in the novel intermediate site coordinated by Glu^{173} (24 Ca^{2+} ions). The three calcium ion binding sites, around the 3-fold symmetry axes, ferroxidase sites, and novel intermediate sites coordinated by the Glu^{173}, are shown in Fig. 3*a*.

Calcium ions on the outer surface of the ferritin shell had seven coordinated waters, two of which were hydrogen bonded to the carboxylate oxygen atoms of Asp^{43} and Glu^{46}, and one of which was hydrogen bonded to the acetate anion located between the side chains of Arg^{38} and Lys^{108}. The acetate anions were also usually hydrogen bonded to the main chain nitrogen of Ser^{35}. These outer calcium ions were not related to the intermolecular contact, in contrast to vertebrate ferritin (4–7). Intermolecular contacts were formed mainly by hydrogen bonds or salt bridges between the main chains or side chains of residues positioned around the end of the C-helix (Ser^{152}, Thr^{155}, Lys^{156}, and Asn^{157}) and the side chains of Lys^{40}, Asp^{43}, Glu^{44}, and Ser^{47} positioned around the start of the A-helix.

3-Fold Symmetry Axis—The hydrophilic channel penetrating along the 3-fold symmetry axis is considered the iron entry channel to the inner cavity of the ferritin shell (8–11). The channel of soybean ferritin, SFER4, had similar coordination with mammalian ferritins. As for the 3-fold channel of SFER4, the channel is lined with Asp^{164}, Glu^{167}, and Thr^{168} of three symmetrically related subunits (Fig. 3*a*, residues shown in *yellow*), corresponding to Asp^{131}, Glu^{134}, and Thr^{135} of the human H chain. In the crystal structure of SFER4, two electronic densities of calcium ions are found around the 3-fold symmetry axis in the bottleneck of the funnel-like channel leading to the cavity. One calcium ion positioned deeper inside the 3-fold symmetry channel is coordinated by OEs in the side chains of two symmetrically related Glu^{167}, one OD of Asp^{164} and three waters (Fig. 3*b*). On the other hand, the other calcium ion, positioned outside the channel, is coordinated by an OE of Glu^{167} and three to four waters. The structure around the 3-fold channel composed of chain L, M, and T was unambiguously determined, whereas the outer calcium ions and its ligands in other channels were sometimes disordered. In the channel composed of chains L, M, and T, the inner calcium ion was coordinated by two ODs of Asp^{164} in chains L and T, two OEs of Glu^{167} in chains L and M, and three waters. On the other hand, the outer calcium is coordinated by two OEs of Glu^{167} of chains L and M plus four coordinated waters (Fig. 3*b*).

4-Fold Symmetry Axis—The E-helices of vertebrate ferritins lie roughly parallel with the 4-fold axis, making a hydrophobic channel traverse the shell. In the homo 24-mer of human H and L chains, this channel is formed by three layers. In the case of the H chain, the inner chain is lined with four histidines, whereas the middle and outer chains are each lined with four leucines. On the other hand, the channel in the human L chain is lined with 12 leucines, making it highly hydrophobic. In contrast, this channel in plant ferritin SFER4 is formed by histidine side chains (Fig. 4*a*) composed of two layers (Fig. 4*b*), because the side chain of Met^{203}, which corresponds to the His^{173} or Leu^{169} positions in the inner layer of the human H chain or L chain, does not form the inner layer of the 4-fold channel. The two layers of SFER4 are composed of two histidines (His^{195} and His^{199}) and their 4-fold symmetry related mates (Fig. 4*b*). Thus, the channel is lined by eight histidines. The NDs in the side chains of outer histidines (His^{195}) are directed to the outer surface of the 4-fold channel, whereas the NEs of His^{195} electrostatically interact with the NDs of the inner histidine (His^{199}) in a symmetrically related subunit (Fig. 4*b*). Consequently, the NEs of inner histidines are directed to the inner cavity of the protein shell. The distance between the two nitrogen atoms in histidine side chains is ~2.9 Å. No electronic peaks of metal ion are seen around the channel, in contrast to other kinds of ferritins (17, 56).

Deduced Ferroxidase Center and Nucleation Center—In general, the ferroxidase center, located inside the four-helix bundle of each subunit, contains two metal binding sites, named A and B. It was suggested that the occupancy of site A is higher than that of site B (4). Concerning the SFER4, the ferroxidase center is composed of Glu^{56}, Tyr^{63}, Glu^{91}, His^{94}, Glu^{140}, and Gln^{174}, corresponding to Glu^{27}, Tyr^{34}, Glu^{62}, His^{65}, Glu^{107}, and Gln^{141}, respectively, of the human H chain ferritin (Fig. 1). In the native crystal structure of SFER4, metal binding was seen only in site A, although all amino acid residues of the ferroxidase center are conserved and the overall structure of this site is nearly identical. The metal binding site A is coordinated by Glu^{56}, Glu^{91}, His^{94}, and three waters (Fig. 5*a*), showing that the coordination of calcium ion in this site is nearly identical with metal binding site A of the human H chain.

The putative nucleation center of SFER4 is composed of glutamates facing the inner cavity, Glu^{86}, Glu^{89}, Glu^{90}, and Glu^{93},

FIGURE 2. **Ribbon diagram of the plant ferritin, SFER4.** *a* and *b*, the whole oligomer viewed down a 3-fold and a 4-fold symmetry axis, respectively. The N-terminal extension peptide forms a loop and a short helix lies on the neighboring 3-fold symmetry mate subunit. *c*, stereoview of a superimposition of the soybean ferritin SFER4 subunit (*blue*) on the human ferritin H chain (*red*, PDB accession code 2FHA).

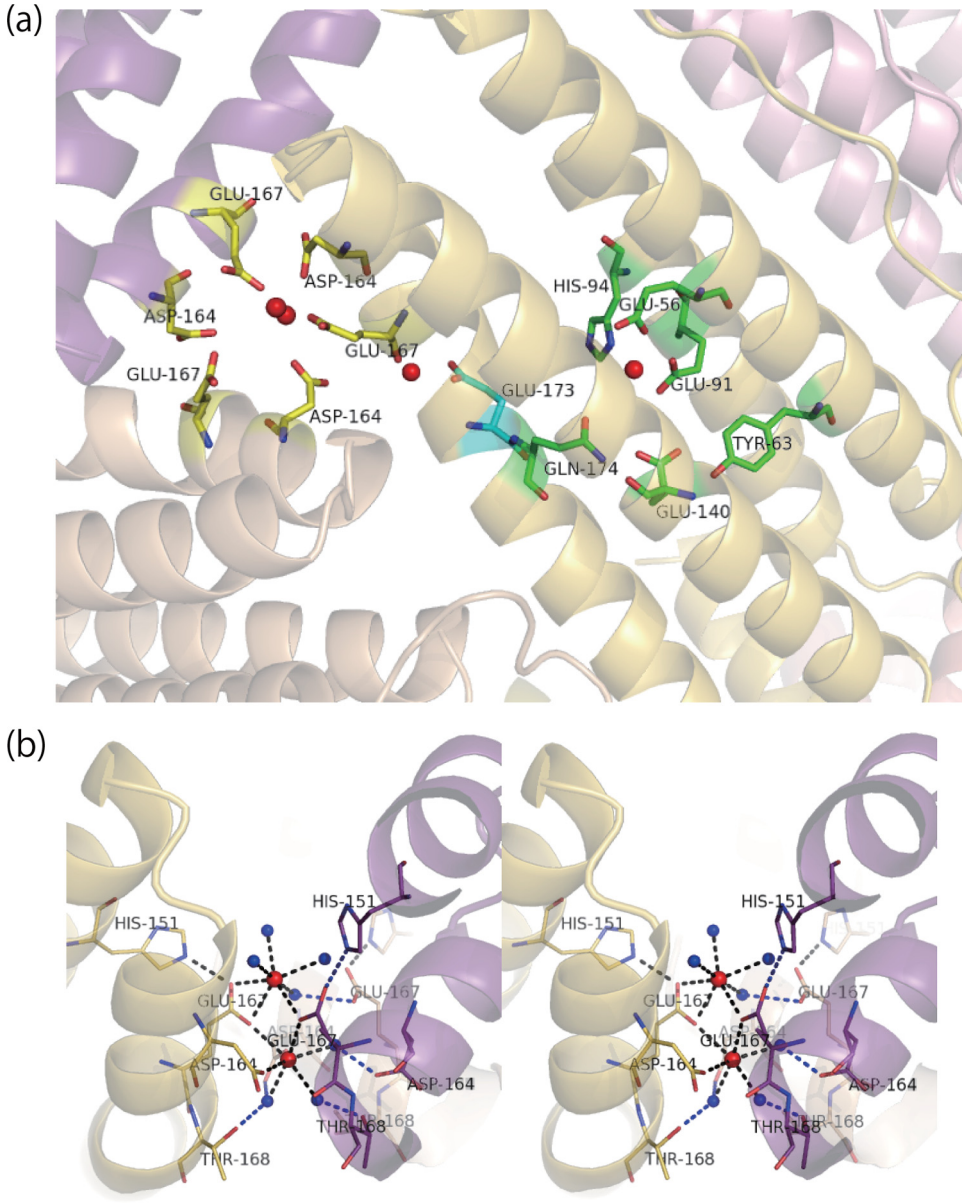

FIGURE 3. *a*, positions of the three calcium binding sites, 3-fold symmetry axis, ferroxidase site, and novel intermediate site coordinated by Glu^{173} in the ferritin shell. The calcium atoms are shown as *red balls*. Residues forming a metal binding site of the 3-fold axis, a novel "transit site," and ferroxidase center are shown in *yellow*, *cyan*, and *green*, respectively. *b*, the structure of the deduced metal ion entry channel penetrating along the 3-fold symmetry axis and metal binding site in the channel. This channel is lined with hydrophilic side chains of Asp^{164}, Glu^{167}, and Thr^{168}, and two calcium ions per channel are seen (in *red*). Waters ligated to the calcium ions or hydrogen bonded to the side chains are shown in *blue*. *Blue broken lines*, hydrogen bonds; *black broken lines*, metal coordination bonds. The channels formed by chain L (shown in "*yellow*"), M (*purple*), and T (*beige*) are represented from the view perpendicular to the axis (stereo view).

corresponding to Glu^{53}, Glu^{56}, Glu^{57}, and Glu^{60} of the human L chain (Fig. 1). In the present model Glu^{90} has an alternative conformation, and these four residues tend to be disordered, as seen in crystallographic analysis of other L chains. The electron densities with high intensity (8 to 10 σ) are seen in the vicinity of the side chains of Glu^{93} and Glu^{96}. Some of the peaks exhibited weak anomalous signals; therefore, they were considered calcium ions. In addition to these residues, Asp^{71}, Glu^{86}, Glu^{89}, Glu^{90}, Glu^{100}, Glu^{169}, Glu^{173}, Glu^{176}, and Glu^{183} are also facing the inner cavity, rendering it acidic. Calcium ions are also seen in the vicinity of Glu^{183}, Asp^{71}, and Lys^{179}, all of which are facing the inner cavity.

Novel Metal Binding Site—A novel metal binding site is seen intermediate between the channel and ferroxidase center binding sites 3-fold. The site, which is positioned at the bottom of the 3-fold symmetry channel and facing the inner cavity of the ferritin shell, is coordinated by the OE of Glu^{173}, carbonyl oxygen of Thr^{168}, and four waters (Fig. 6). The distances from two OEs of Glu^{173} and the carboxyl oxygen of Thr^{168} are 2.48, 2.53, and 2.32 Å. This calcium ion binding site is seen clearly in all chains of the SFER4 crystal structure. The distance of this calcium ion from the inner calcium ion in the 3-fold symmetry axis is 9.7 Å, whereas that from the ferroxidase site A is 12.4 Å.

Biochemical Property of the E173A Mutant—To assess the function of the Glu^{173} residue of SFER4, the E173A mutant, in which Glu^{173} was replaced with alanine, was prepared by the *E. coli* expression system, and ferroxidase/nucleation activity was compared with the native SFER4. The proper oligomeric formation of the E173A mutant was verified by gel filtration (data not shown). UV spectral absorption around 305–330 nm has been traditionally used to monitor the ferroxidase activity of ferritins. When adding ferrous ions to ferritin possessing a ferroxidase center such as the human H chain, the absorbance around 310 nm, which is characteristic of μ-oxo-bridged Fe(III) dimers (21, 57), increases as a result of the Fe(II) oxidation. Fig. 7 shows the time-dependent change in absorbance at 310 nm, when ferrous ions were added to SFER4 and the E173A mutant at molar ratios of 1:20 (20 μM ferrous ions was added to 1 μM of the SFER4 and E173A) (Fig. 7*a*) and 1:100 (Fig. 7*b*). The results show delays in the formation of the μ-oxo-bridged Fe(III) species in the E173A mutant compared with SFER4 in all conditions tested here at ferritin/iron ratios of 1:20, 1:40, and 1:100, whereas the final absorbencies were nearly identical (Fig. 7). The kinetic parameters were calculated as follows: K_m(SFER4) = 31.9 μM, K_m(E173A) = 69.6 μM, V_{max}(SFER4) = 0.525 μM/s, V_{max}(E173A) = 0.508 μM/s, K_{cat}(SFER4) = 0.525/s, and K_{cat}(E173A) = 0.508/s. The E173A mutant exhibited a specificity constant (K_{cat}/K_m) 2.27-fold decrease compared with the value of the SFER4.

DISCUSSION

Since 1991, when the three-dimensional structure of human H-type ferritin was solved (4), many structures of ferritin from various species have been investigated and iron storage mechanisms have been proposed. In the present study, we reported the three-dimensional structural model and novel metal binding site of plant ferritin from soybean. The results showed that the overall structure of plant ferritin, SFER4, was highly conserved among known structures of ferritins. It was proved that part of the plant-specific EP formed a loop and a short helix, although this region was highly disordered. This observation supports the prediction by Lobréaux *et al.* (42) that this region of pea ferritin would form a short helix named the P-helix, and it would lie on the outer surface of the assembled ferritin shell. They also predicted that the P-helix was folded back to the surface of the original subunit. However, the present model shows that this N-terminal helix is interacting with a neighboring subunit on the shell surface (see Fig. 2 and Table 2). It has been suggested that the N-terminal EP stabilizes the whole oligomeric conformation of plant ferritin (39–41). The interactions between the EP and the shell surface were formed mainly via apolar contacts. The model demonstrates that seven residues contribute to the interactions, in which four residues (Leu^{135}, Leu^{139}, Leu^{142}, and Lys^{146}) are members of the C-helix (Table 2). Thus, it can be considered that the EP stabilizes the protein shell by maintaining the conformation of the C-helix. It has been suggested that interaction between the conserved Leu^{110} in the C-helix and Leu^{134} in the D-helix of the bullfrog H chain, which correspond to Leu^{147} and Leu^{171} of SFER4 (Fig. 1), plays a crucial role in stabilization of the 3-fold channel and that the mutation of these residues enhances the iron release from the ferritin mineral core (58–60). The EP may contribute to tight packing of the 3-fold pore conformation by stabilizing the C-helix. This hypothesis is based on the faster rate of iron incorporation of plant ferritin with EP deletion than that of the native protein (40). It is possible that the removal of EP accelerates not only the rate of iron incorporation but also that of iron release from the ferritin shell. Concerning the function of the EP, Li *et al.* (61) recently suggested that the EP has iron binding capacity and facilitates iron incorporation into the ferritin shell. However, there is no metal binding site in the EP of the present

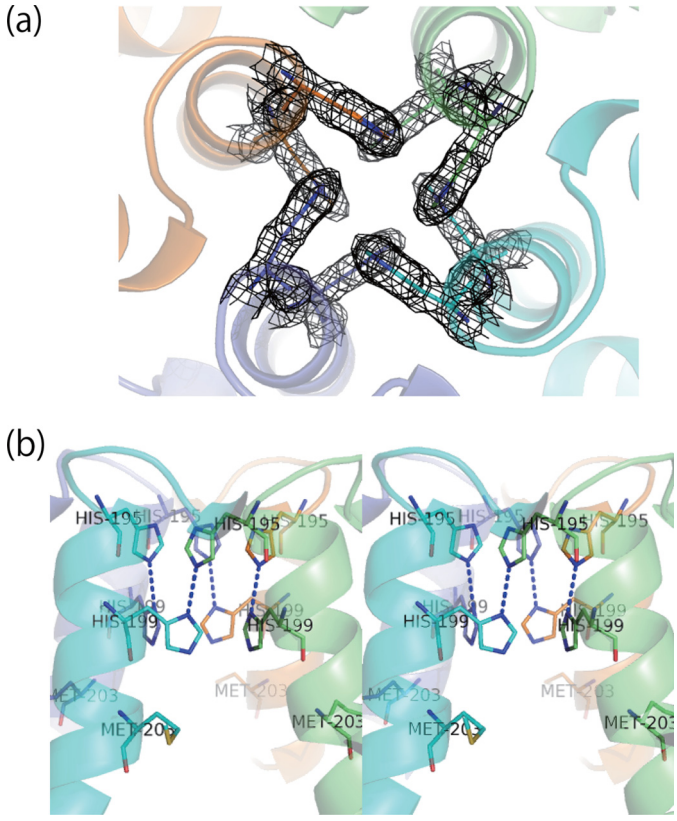

FIGURE 4. **Inter-subunit interactions around the 4-fold symmetry axis of the SFER4.** The channels are represented with two different orientations: (*a*) aligned on the 4-fold axis and (*b*) perpendicular to the axis (stereo view). The electron densities of the four lined histidines contoured at 1.5 σ are shown as a mesh in *a*. *Blue broken lines*, electrostatic interaction of histidine side chains.

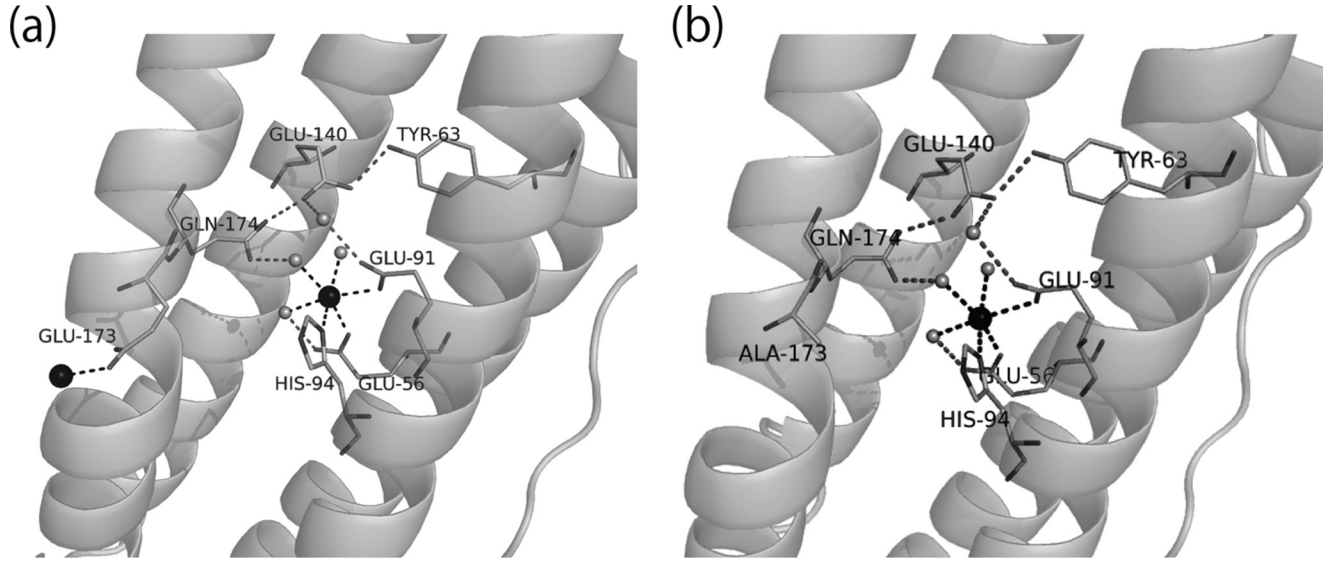

FIGURE 5. **Metal binding site in the ferroxidase center of the SFER4 (*a*) and its variant E173A (*b*).** A metal binding site positioned near the center (described below) is also shown *a*. The atom color code is *black* for calcium and *gray* for oxygen of water. *Gray broken lines*, hydrogen bonds; *black broken lines*, metal coordination bonds.

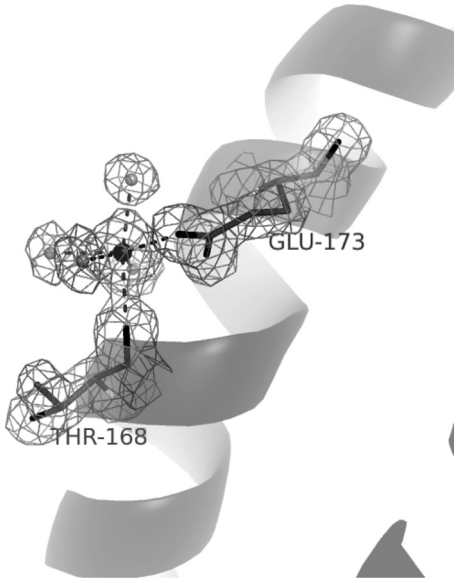

FIGURE 6. **A novel metal binding site coordinated by Glu^{173}.** A novel metal binding site is represented by coordination residues, Glu^{173} and Thr^{168}, with the electron density ($2|F_o| - |F_c|$) contoured at 1.5σ shown as a mesh. The atom color code is *black* for calcium and *gray* for oxygen of water. *Black broken lines* indicate the metal coordination bonds.

SFER4 model. To elucidate the function of EP in iron binding, structural analysis of a iron derivative of plant ferritin is required. However, we have not yet obtained crystals of the plant ferritins soaked with iron.

Another unique feature of plant ferritin is its 4-fold symmetry channel. The present model of SFER4 indicates that this narrow channel is lined with eight tightly packed histidine side chains, resulting in formation of a hydrogen bond network from inside to outside the ferritin shell (Fig. 4). In contrast, in mammalian ferritins the channel is lined with 12 leucines or 8 leucines plus 4 histidines (4, 5). Takahashi and Kuyucak (62) suggested that the 4-fold channel functions as a proton channel that facilitates hydrogen ion transfer in and out of the human H ferritin shell. As a result of the ferroxidase reaction, the proton concentration in the inner cavity increases, which leads to protonation of NEs of the His^{199} side chain facing the inner cavity. The proton can be transferred by sequential protonation/deprotonation of His^{199} and His^{195} side chains to be exported from the shell. Thus, from a structural point of view, it can be considered that the 4-fold symmetry axis of plant ferritin is more feasible than that of the mammalian ferritin if this channel functions as a pathway for proton transfer. The histidine residues (His^{195} and His^{199}) lining the channel are highly conserved among plant ferritins, suggesting that the histidine cluster forming the 4-fold channel is a common feature of plant ferritin species.

The structures of the key sites for the iron storage process of ferritin, the 3-fold iron entry channel, the ferroxidase center, and the nucleation center were proven to be highly conserved among the SFER4 and vertebrate ferritins. In the present model of SFER4, metal binding in the ferroxidase site was seen only in site A (see Fig. 5*a*). In general, the ferroxidase center is composed of two metal binding sites, A and B (4, 5, 63). However, x-ray crystallographic analysis of non-heavy atom derivatives

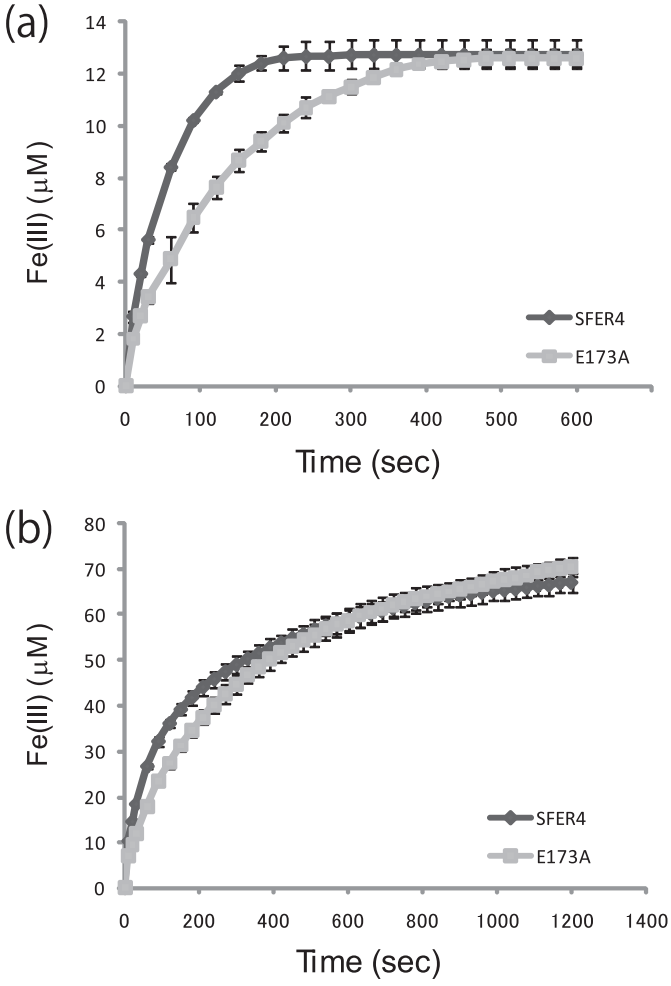

FIGURE 7. **Effect of E173A mutation on iron oxidation rates of plant ferritin SFER4.** Progress curves of μ-oxo-bridged Fe(III) generation monitored at 310 nm upon the addition of ferrous iron sulfate ammonium to the SFER4 and its E173A variant at a protein concentration of 1 μM and iron concentrations of 20 (*a*) and 100 (*b*) μM. The formation of μ-oxo-bridged Fe(III) was calculated from absorbance at 310 nm. Data are given as the mean ± S.D. of at least three individual experiments.

indicated that site B was sometimes vacant and that an alkaline-earth metal such as calcium or magnesium bound only to site A (56, 57). Because many studies concerning ferroxidase activity of plant ferritin have suggested that plant ferritin species have ferroxidase activity comparable with that of mammalian or bacterial ferritin (30, 40, 64), the ferroxidase site of SFER4 can be considered functional.

Recently, the roles of the carboxyl side chains facing the inner cavity of ferritins have been discussed. It was suggested that the acidic side chains play a critical role in Fe(III) nucleation on the cavity surface (14, 65, 66). In contrast, Bou-Abdallah *et al.* (67) demonstrated that the core formation rate was not affected by deletion of the inner glutamate residues (Glu^{64} and Glu^{67}), which were considered the nucleation site of human H ferritin. In the present model of SFER4, in addition to the traditional nucleation site Glu^{93}/Glu^{96}, a calcium ion was seen in the vicinity of Asp^{71} and Glu^{183} facing the inner cavity. Asp^{71} and Glu^{183} of SFER4 correspond to Asp^{42} and Asp^{150} of the human H chain (Fig. 1). It is possible that this site functions as the second nucleation site for Fe(III) core formation and that the traditionally

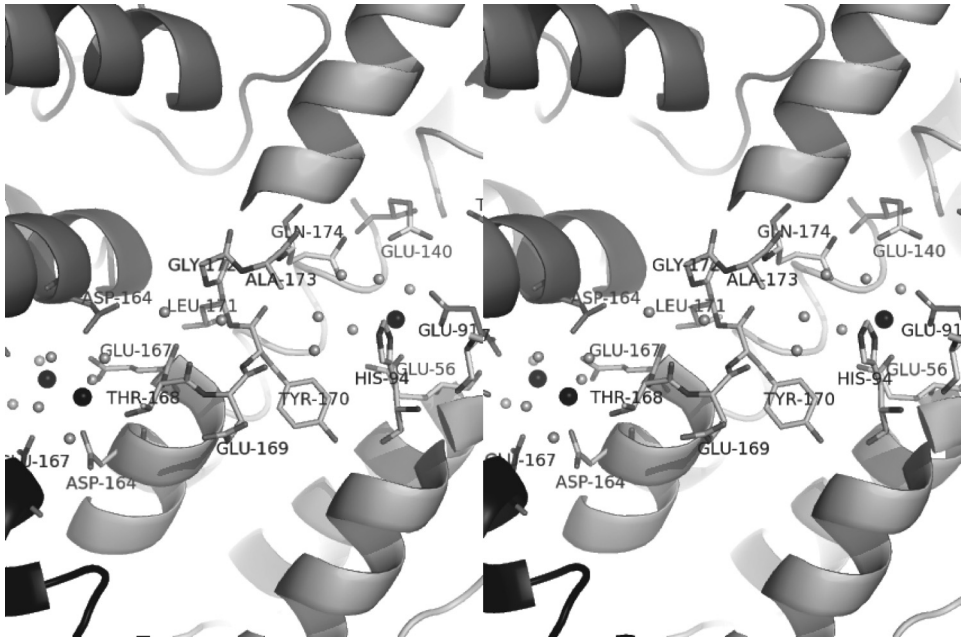

FIGURE 8. **The hydrophilic route from the 3-fold channel to the ferroxidase site of the E173A variant (stereo view).** This figure is the view from the inner cavity side. The ferroxidase site (Glu^{56}, Glu^{91}, His^{94}, Glu^{140}, and Gln^{174}) of chain G and the 3-fold channel composed of chains G, F, and O of the E173A variant are illustrated. The 3-fold channel is lined with Asp^{164} and Glu^{167} of the three chains (*left side*). The hydrophilic route emerged because of the substitution (E173A) and the kink of the D-helix in Tyr^{170}. The calcium atoms and water molecules are shown as *black* and *gray balls*, respectively.

identified nucleation site is not the sole nucleation site. In fact, these residues, Asp^{42} and Asp^{150}, were maintained in the experiments performed by Bou-Abdallah (67). Furthermore, Levi *et al.* (14) suggested that disruption of Asp^{42} was required to abolish the iron incorporation activity of human H chain ferritin. These observations also support the hypothesis that the putative nucleation site is not the sole nucleation site. The contribution of each acidic side chain on the cavity surface should be determined.

The pathway from the iron entry channel via the ferroxidase center to the nucleation site has been investigated by x-ray crystallographic analysis and site-directed mutagenesis (4, 7, 56, 68, 69). In the present SFER4 model, two calcium ions were seen around the iron entry channel (Fig. 3*b*), showing that amino acid residues related to the coordination with calcium ions were Asp^{164} and Glu^{167}, which correspond to Asp^{131} and Glu^{134} of human H chain, and to Asp^{127} and Glu^{130} of human L chain, respectively (Fig. 1). Grainer *et al.* (68) suggested that the alternative conformation of Asp^{127} and Glu^{130} in the human L chain were important in assisting the metal movement from outside to inside through the channel. Similarly, Toussaint *et al.* (56) observed metal binding to Cys^{130} positioned at the entrance to the 3-fold channel and suggested that the alternative configuration of this residue facilitated metal entry into the channel. As for the movement from the ferroxidase site to the nucleation site, x-ray crystallographic analysis of human H chain has shown that Glu^{61} had an alternative conformation and served to transport metal ions from the ferroxidase site to the nucleation site (4, 5). Furthermore, Stillman *et al.* (7) indicated that the alternative conformation of His^{46} of ferritin from *E. coli* (EcFTN), which is a highly conserved amino acid residue among prokaryotic ferritin, enabled the metal to move from the ferroxidase center. In the present model of plant ferritin SFER4, a novel metal binding site, Glu^{173}, was discovered between the two well defined metal binding sites: the iron entry channel and the ferroxidase site (Fig. 3*a*). To date, few studies have described the pathway from the metal binding site in the 3-fold channel to the ferroxidase center. We postulate that this residue, Glu^{173} of the SFER4, functions as a transit site from the metal entrance to the ferroxidase site. This assumption was supported by the difference in ferroxidase activity of native SFER4 and the E173A mutant, whose ferroxidase site was not disrupted by the mutation (Fig. 5*b*). The K_m value for iron oxidation of the mutant was increased to 2.2-fold compared with that of native SFER4. The delay in iron oxidation in the E173A mutant was more prominent at low iron concentrations (ferritin/iron = 1:20) (Fig. 7*a*), whereas the difference in activity diminished as the iron concentration increased (ferritin/iron = 1:100) (Fig. 7*b*). These results, together with the fact that Glu^{173} is not involved in iron oxidation in the ferroxidase site (Fig. 5*a*), indicate that the side chain of this residue is required for mechanical transfer of the metal ions from the entry channel to the ferroxidase site, especially under ordinary physiological conditions *in vivo*. For instance, iron atoms enter from the 3-fold channels and interact with Glu^{167} and/or Asp^{164} and are then translocated from Asp^{164} or Thr^{168} to Glu^{173}. In the crystal structure of native SFER4, calcium ions are seen coordinated by the side chain of Glu^{173} and the main chain oxygen of Thr^{168} (Fig. 6). In another orientation, the side chain of Glu^{173} can interact with the side chains of Gln^{174} and His^{94}, which are part of the ferroxidase site of SFER4. On the other hand, in the crystal structure of the E173A variant, no metal ion was seen adjacent to Ala^{173}. But, a hydrophilic route emerged between Thr^{168} (deep in the entry channel) and the ferroxidase site. This hydrophilic route crossing the D-helix is positioned on the main chain oxygen of Thr^{168} and Glu^{169}, which do not hydrogen bond with the main chain nitrogen of Gly^{172} and Ala^{173} because of the kink in the D-helix (Tyr^{170}) (Fig. 8). This hydrophilic route of the mutant may enable the diffusion of metal ions from the entry channel to the ferroxidase site, especially in the presence of a high concentration of metal ions (Fig. 7*b*).

The Glu^{173} of SFER4 is conserved not only among all known members of plant ferritins such as soybean, pea, maize, tobacco, and *Arabidopsis* (22, 25, 28, 30, 44), but also among ferritins from eukaryotes, except the mouse L chain ferritin (Fig. 1). In the well characterized structure of human H ferritin, conformation around Glu^{140} (Glu^{173} of the SFER4) is nearly identical to that of SFER4. Therefore, Glu^{140} of human H ferritin can also

contribute to the mechanical transfer of metal ions. However, further investigation into the function of the glutamate residue using vertebrate ferritins is required. In prokaryotic ferritin, this glutamate residue is also conserved in non-heme binding bacterial ferritin, such as EcFTN (from *E. coli*) (Fig. 1). In contrast, the corresponding glutamate is substituted with a lysine (Lys^{140}) in the mouse L chain. Santanbrogio *et al.* (53) suggested that this substitution causes the low iron incorporation activity of the mouse L chain compared with the human L chain, which has a Glu^{140}, corresponding to the Glu^{173} of SFER4. This observation also supports the significance of the Glu^{173} side chain in iron traffic in ferritin.

Thus, it is possible that the function of this residue, Glu^{173} of SFER4, as a transit site from the iron entry channel to the ferroxidase site, is related to a universal mechanism in iron translocation in ferritin. This finding provides evidence that a common pathway does exist from the iron entry channel to the ferroxidase center in ferritin molecules in various living kingdoms.

Acknowledgments—We thank Prof. Evelyn M. Tecson-Mendoza (University of the Philippines, Los Banos) for critical reading of the manuscript. The synchrotron radiation experiments were performed at the BL44XU and BL38B1 in the SPring-8 with the approval of the Japan Synchrotron Radiation Research Institute (JASRI) (proposal numbers 2008B6828 and 2009A1249).

REFERENCES

1. Harrison, P. M., and Arosio, P. (1996) *Biochim. Biophys. Acta* **1275,** 161–203
2. Theil, E. C. (1987) *Annu. Rev. Biochem.* **56,** 289–315
3. Arosio, P., Ingrassia, R., and Cavadini, P. (2009) *Biochim. Biophys. Acta* **1790,** 589–599
4. Lawson, D. M., Artymiuk, P. J., Yewdall, S. J., Smith, J. M., Livingstone, J. C., Treffry, A., Luzzago, A., Levi, S., Arosio P., Cesareni, G., Thomas, C. D., Shaw, W. V., and Harrison, P. M. (1991) *Nature* **349,** 541–544
5. Hempstead, P. D., Yewdall, S. J., Fernie, A. R., Lawson, D. M., Artymiuk, P. J., Rice, D. W., Ford, G. C., and Harrison, P. M. (1997) *J. Mol. Biol.* **268,** 424–448
6. Granier, T., Comberton, G., Gallois, B., d'Estaintot, B. L., Dautant, A., Crichton, R. R., and Précigoux, G. (1998) *Proteins* **31,** 477–485
7. Stillman, T. J., Hempstead, P. D., Artymiuk, P. J., Andrews, S. C., Hudson, A. J., Treffry, A., Guest, J. R., and Harrison, P. M. (2001) *J. Mol. Biol.* **307,** 587–603
8. Stefanini, S., Desideri, A., Vecchini, P., Drakenberg, T., and Chiancone, E. (1989) *Biochemistry* **28,** 378–382
9. Treffry, A., Harrison, P. M., Luzzago, A., and Cesareni, G. (1989) *FEBS Lett.* **247,** 268–272
10. Yablonski, M. J., and Theil, E. C. (1992) *Biochemistry* **31,** 9680–9684
11. Levi, S., Santambrogio, P., Corsi, B., Cozzi, A., and Arosio, P. (1996) *Biochem. J.* **317,** 467–473
12. Arosio, P., Adelman, T. G., and Drysdale, J. W. (1978) *J. Biol. Chem.* **253,** 4451–4458
13. Leibold, E. A., Aziz, N., Brown, A. J., and Munro, H. N. (1984) *J. Biol. Chem.* **259,** 4327–4334
14. Levi, S., Yewdall, S. J., Harrison, P. M., Santambrogio, P., Cozzi, A., Rovida, E., Albertini, A., and Arosio, P. (1992) *Biochem. J.* **288,** 591–596
15. Lawson, D. M., Treffry, A., Artymiuk, P. J., Harrison, P. M., Yewdall, S. J., Luzzago, A., Cesareni, G., Levi, S., and Arosio, P. (1989) *FEBS Lett.* **254,** 207–210
16. Levi, S., Luzzago, A., Cesareni, G., Cozzi, A., Franceschinelli, F., Albertini, A., and Arosio, P. (1988) *J. Biol. Chem.* **263,** 18086–18092
17. Ha, Y., Shi, D., Small, G. W., Theil, E. C., and Allewell, N. M. (1999) *J. Biol. Inorg. Chem.* **4,** 243–256
18. Hamburger, A. E., West, A. P., Jr., Hamburger, Z. A., Hamburger, P., and Bjorkman, P. J. (2005) *J. Mol. Biol.* **349,** 558–569
19. Frolow, F., Kalb, A. J., and Yariv, J. (1994) *Nat. Struct. Biol.* **1,** 453–460
20. Chasteen, N. D., and Harrison, P. M. (1999) *J. Struct. Biol.* **126,** 182–194
21. Yang, X., Chen-Barrett, Y., Arosio, P., and Chasteen, N. D. (1998) *Biochemistry* **37,** 9743–9750
22. Lobreaux, S., Massenet, O., and Briat, J. F. (1992) *Plant Mol. Biol.* **19,** 563–575
23. Wicks, R. E., and Entsch, B. (1993) *Biochem. Biophys. Res. Commun.* **192,** 813–819
24. Wardrop, A. J., Wicks, R. E., and Entsch, B. (1999) *Biochem. J.* **337,** 523–530
25. Petit, J. M., Briat, J. F., and Lobréaux, S. (2001) *Biochem. J.* **359,** 575–582
26. Masuda, T., Goto, F., and Yoshihara, T. (2001) *J. Biol. Chem.* **276,** 19575–19579
27. Strozycki, P. M., Skapska, A., Szcześniak, K., Sobiezcruzuk, E., and Briat, J. F. (2003) *Physiol. Plant.* **118,** 380–389
28. Jiang, T. B. (2005) *J. Integr. Plant Biol.* **47,** 477–486
29. Dong, X., Sun, Q., Wei, D., Li, J., Li, J., Tang, B., Jia, Q., Hu, W., Zhao, Y., and Hua, Z. C. (2007) *FEBS Lett.* **581,** 5796–5802
30. Li, C., Hu, X., and Zhao, G. (2009) *Biochimie* **91,** 230–239
31. Fobis-Loisy, I., Loridon, K., Lobréaux, S., Lebrun, M., and Briat, J. F. (1995) *Eur. J. Biochem.* **231,** 609–619
32. Lescure, A. M., Proudhon, D., Pesey, H., Ragland, M., Theil, E. C., and Briat, J. F. (1991) *Proc. Natl. Acad. Sci. U.S.A.* **88,** 8222–8226
33. Gaymard, F., Boucherez, J., and Briat, J. F. (1996) *Biochem. J.* **318,** 67–73
34. Savino, G., Briat, J. F., and Lobréaux, S. (1997) *J. Biol. Chem.* **272,** 33319–33326
35. Wei, J., and Theil, E. C. (2000) *J. Biol. Chem.* **275,** 17488–17493
36. Petit, J. M., van Wuytswinkel, O., Briat, J. F., and Lobréaux, S. (2001) *J. Biol. Chem.* **276,** 5584–5590
37. Briat, J. F., Laboure, A. M., Laulhère, J. P., Lescure, A. M., Lobréaux, S., Pesey, H., Proudhon, D., and Wuytswinkel, O. (1995) in *Iron Nutrition in Soils and Plants* (Abadía, J., ed) pp. 265–276, Kluwer Academic Publishers, Dordrecht, The Netherlands
38. Ragland, M., Briat, J. F., Gagnon, J., Laulhere, J. P., Massenet, O., and Theil, E. C. (1990) *J. Biol. Chem.* **265,** 18339–18344
39. Laulhere, J. P., Laboure, A. M., and Briat, J. F. (1989) *J. Biol. Chem.* **264,** 3629–3635
40. van Wuytswinkel, O., Savino, G., and Briat, J. F. (1995) *Biochem. J.* **305,** 253–261
41. van Wuytswinkel, O., and Briat, J. F. (1995) *Biochem. J.* **305,** 959–965
42. Lobreaux, S., Yewdall, S. J., Briat, J. F., and Harrison, P. M. (1992) *Biochem. J.* **288,** 931–939
43. Masuda, T., Mikami, B., Goto, F., Yoshihara, T., and Utsumi, S. (2003) *Biochim. Biophys. Acta* **1645,** 113–115
44. Masuda, T., Goto, F., Yoshihara, T., Ezure, T., Suzuki, T., Kobayashi, S., Shikata, M., and Utsumi, S. (2007) *Protein Expr. Purif.* **56,** 237–246
45. Pace, C. N., Vajdos, F., Fee, L., Grimsley, G., and Gray, T. (1995) *Protein Sci.* **4,** 2411–2423
46. Otwinowski, Z., and Minor, W. (1997) *Methods Enzymol.* **276,** 307–326
47. Vagin, A., and Teplyakov, A. (1997) *J. Appl. Cryst.* **30,** 1022–1025
48. Potterton, E., Briggs, P., Turkenburg, M., and Dodson, E. (2003) *Acta Crystallogr. D Biol. Crystallogr.* **59,** 1131–1137
49. Murshudov, G. N., Vagin, A. A., and Dodson, E. J. (1997) *Acta Crystallogr. D Biol. Crystallogr.* **53,** 240–255
50. Emsley, P., and Cowtan, K. (2004) *Acta Crystallogr. D Biol. Crystallogr.* **60,** 2126–2132
51. Adams, P. D., Grosse-Kunstleve, R. W., Hung, L. W., Ioerger, T. R., McCoy, A. J., Moriarty, N. W., Read, R. J., Sacchettini, J. C., Sauter, N. K., and Terwilliger, T. C. (2002) *Acta Crystallogr. D Biol. Crystallogr.* **58,** 1948–1954
52. Chasteen, N. D., and Theil, E. C. (1982) *J. Biol. Chem.* **257,** 7672–7677
53. Santambrogio, P., Cozzi, A., Levi, S., Rovida, E., Magni, F., Albertini, A., and Arosio, P. (2000) *Protein Expr. Purif.* **19,** 212–218
54. Pâgues, E., Pâques, A., and Crichton, R. R. (1980) *Eur. J. Biochem.* **107,** 447–453

55. Zhao, G., Bou-Abdallah, F., Arosio, P., Levi, S., Janus-Chandler, C., and Chasteen, N. D. (2003) *Biochemistry* **42,** 3142–3150
56. Toussaint, L., Bertrand, L., Hue, L., Crichton, R. R., and Declercq, J. P. (2007) *J. Mol. Biol.* **365,** 440–452
57. Langlois d'Estaintot, B., Santambrogio, P., Granier, T., Gallois, B., Chevalier, J. M., Précigoux, G., Levi, S., and Arosio, P. (2004) *J. Mol. Biol.* **340,** 277–293
58. Jin, W., Takagi, H., Pancorbo, B., and Theil, E. C. (2001) *Biochemistry* **40,** 7525–7532
59. Liu, X., Jin, W., and Theil, E. C. (2003) *Proc. Natl. Acad. Sci. U.S.A.* **100,** 3653–3658
60. Theil, E. C., Liu, X. S., and Tosha, T. (2008) *Inorg. Chim. Acta* **361,** 868–874
61. Li, C., Fu, X., Qi, X., Hu, X., Chasteen, N. D., and Zhao, G. (2009) *J. Biol. Chem.* **284,** 16743–16751
62. Takahashi, T., and Kuyucak, S. (2003) *Biophys. J.* **84,** 2256–2263
63. Liu, X., and Theil, E. C. (2004) *Proc. Natl. Acad. Sci. U.S.A.* **101,** 8557–8562
64. Laulhere, J. P., and Briat, J. F. (1993) *Biochem. J.* **290,** 693–699
65. Yang, C. Y., Meagher, A., Huynh, B. H., Sayers, D. E., and Theil, E. C. (1987) *Biochemistry* **26,** 497–503
66. Levi, S., Santambrogio, P., Cozzi, A., Rovida, E., Corsi, B., Tamborini, E., Spada, S., Albertini, A., and Arosio, P. (1994) *J. Mol. Biol.* **238,** 649–654
67. Bou-Abdallah, F., Biasiotto, G., Arosio, P., and Chasteen, N. D. (2004) *Biochemistry* **43,** 4332–4337
68. Granier, T., Langlois d'Estaintot, B., Gallois, B., Chevalier, J. M., Précigoux, G., Santambrogio, P., and Arosio, P. (2003) *J. Biol. Inorg. Chem.* **8,** 105–111
69. Stillman, T. J., Connolly, P. P., Latimer, C. L., Morland, A. F., Quail, M. A., Andrews, S. C., Treffry, A., Guest, J. R., Artymiuk, P. J., and Harrison, P. M. (2003) *J. Biol. Chem.* **278,** 26275–26286